Molecular Biology of the Cell
Vol. 12, 2378–2395, August 2001

Filopodial Initiation and a Novel Filament-organizing Center, the Focal Ring

Michael Steketee, Kenneth Balazovich, and Kathryn W. Tosney*

Department of Biology and Neuroscience Program, The University of Michigan, Ann Arbor, Michigan 48109

Submitted July 3, 2000; Revised March 6, 2001; Accepted May 31, 2001
Monitoring Editor: Paul T. Matsudaira

This study examines filopodial initiation and implicates a putative actin filament organizer, the focal ring. Filopodia were optically recorded as they emerged from veils, the active lamellar extensions of growth cones. Motile histories revealed three events that consistently preceded filopodial emergence: an influx of cytoplasm into adjacent filopodia, a focal increase in phase density at veil margins, and protrusion of nubs that transform into filopodia. The cytoplasmic influx probably supplies materials needed for initiation. In correlated time lapse-immunocytochemistry, these focal phase densities corresponded to adhesions. These adhesions persisted at filopodial bases, regardless of subsequent movements. In correlated time lapse-electron microscopy, these adhesion sites contained a focal ring (an oblate, donut-shaped structure ~120 nm in diameter) with radiating actin filaments. Filament geometry may explain filopodial emergence at 30 degree angles relative to adjacent filopodia. A model is proposed in which focal rings play a vital role in initiating and stabilizing filopodia: 1) they anchor actin filaments at adhesions, thereby facilitating tension development and filopodial emergence; 2) "axial" filaments connect focal rings to nub tips, thereby organizing filament bundling and ensuring the bundle intersects an adhesion; and 3) "lateral" filaments interconnect focal rings and filament bundles, thereby helping stabilize lamellar margins and filopodia.

INTRODUCTION

Filopodia play a vital role in cellular motility and guidance by sensing the molecular environment, developing adhesions, and transmitting signals that alter cellular motility (e.g., Bastmeyer and Stuermer, 1993; Oakley and Tosney, 1993; Fan and Raper, 1995; Steketee and Tosney, 1999). Filopodia are particularly accessible to study in neuronal growth cones, which are relatively flat, optically favorable structures that regularly extend filopodia. Filopodia are vital to growth cone pathfinding since, without filopodia, a growth cone can still advance but cannot navigate properly (Bentley and Toroian-Raymond, 1986; Chien *et al.*, 1993).

The process of filopodial initiation is the focus of the current study. We refer to filopodial *initiation* as those events that presage filopodial emergence, to filopodial *emergence* as the appearance of a frank filopodium (a cylindrical structure with a relatively constant diameter), and to filopodial *elongation* as the lengthening of emerged filopodia. Filopodial initiation can be closely regulated by environmental interactions. For instance, guidance cues can persistently alter how many filopodia extend (Oakley and Tosney, 1993; Zheng *et al.*, 1996; Steketee and Tosney, 1999) and activating regulators such as protein kinase C can shift motility between filopodial and lamellar states (Rosner and Fischer, 1996).

Filopodial initiation, emergence, and elongation all depend on creating actin filaments, which requires at least three regulated processes: nucleation, elongation, and bundling. Nucleation and elongation are both functions of actin polymerization, but each is separable mechanistically. Nucleation is the creation of free barbed ends, the preferred end for elongation (reviewed in Cooper and Schafer, 2000). Barbed ends may be created by de novo nucleation (Castellano *et al.*, 1999), severing, and/or uncapping existing filaments (reviewed in Stossel *et al.*, 1999), or nucleating from the sides of existing filaments (Mullins *et al.*, 1998, Svitkina and Borisy, 1999). Filaments are then elongated by adding either G-actin monomers to free, barbed ends (reviewed in Stossel *et al.*, 1999) or small filament modules (Tilney *et al.*, 1996b). Elongated filaments are then assembled into larger, more rigid bundles by actin cross-linking proteins (Tilney *et al.*, 1998; reviewed in Bartles, 2000). In many different actin filament-dependent processes, both nucleation and elongation can be regulated by adhesion (Clark *et al.*, 1998) and by interactions with the plasma membrane (reviewed in DeRosier and Tilney, 2000). However, the spatial and temporal mechanisms underlying the nucleation, elongation,

* Corresponding author. E-mail: ktosney@umich.edu.

Table 1. Events associated with filopodial initiation from veils

		Neither supporting filopodium engorged n = 15			One supporting filopodium engorged n = 120			Both supporting filopodia engorged n = 119		
Density	Nub	No.	No. Filo	% Filo	No.	No. Filo	% Filo	No.	No. Filo	% Filo
−	−	1	0	0	5	0	0	6	0	0
+	−	3	0	0	4	0	0	6	0	0
−	+	3	0	0	18	6	38	10	1	10
+	+	8	3	38	93	80	86	97	83	86

A prospective analysis was used to test the degree to which engorgement, focal phase densities, and nubs predicted filopodial emergence from extending veils. The incidence of densities, nubs, and filopodia was charted for 254 veils in 23 growth cones. These veils were further classed as having neither, one, or both supporting filopodia engorged. The table shows the number of veils (#) exhibiting each possible combination of engorgement, densities and nubs, and the number (# filo) and percentage (% filo) of these veils that supported filopodial emergence. For instance, at upper left, only one veil examined lacked all three characteristics, and it failed to support filopodia; at lower right, 97 veils exhibited all three characteristics (both supporting filopodia engorged, and densities and nubs were both present) and 86% of these veils supported emergence. Filopodial emergence was predominantly associated with the presence of all three characteristics, engorgement, a focal phase density, and a nub.

and bundling of filaments during filopodial initiation are poorly understood.

We lack a working model of filopodial initiation. Recent advances support workable models for lamellar extension that have exciting potential for explaining how actin nucleation and polymerization coordinate to extend lamella (Mullins *et al.*, 1998; reviewed in Machesky and Gould, 1999; Svitkina and Borisy, 1999). However, the same mechanisms do not apply to filopodia because they are coordinated by different molecular components and have different cytoskeletal organizations. Molecular studies have identified some components that contribute to filopodial extension generally, such as the Rho family GTPases (reviewed in Hall, 1998). Working models exist for actin filament assembly in a number of actin filament-dependent protrusions, such as the brush border, stereocilium, fly bristle, and acrosomal process (reviewed in DeRosier and Tilney, 2000). However, little is known about the filament dynamics underlying filopodial initiation.

This study develops a working model of filopodial initiation. By examining high-resolution optical recordings, we identified events that consistently precede emerging filopodia: an influx of cytoplasm, a focal increase in phase density, and the protrusion of a nub. The consistency of these features let us identify potential initiation sites before filopodial emergence, and let us detect stable adhesion sites at filopodial bases. When recorded growth cones were examined with immunocytochemistry and electron microscopy, the same sites displayed adhesion components, filament relations, and a novel actin filament organizer, the focal ring. Our study thus begins to distinguish spatial and temporal events that underlie filopodial initiation and develops a testable model for filopodial initiation.

MATERIALS AND METHODS

Cell Culture

Sensory neurons were prepared from dorsal root ganglia removed from chicken embryos (stage 24–25; Hamburger and Hamilton, 1951). Ganglia were washed in neuron media composed of Ham's F12 (Life Technologies, Grand Island, NY) supplemented with 10% heat-inactivated horse serum, antibiotics, hormone additives (Bottenstein *et al.*, 1980), 50 ng/ml nerve growth factor, and 10 mM HEPES, and gently dissociated into explants by pipetting. Small explants (10–15 cells) were plated on polyornithine/laminin-coated glass coverslips in 100-μl wells.

Optical Recording

For recording, cultures were overlaid with mineral oil and maintained at 37°C with a heated stage. Interactions were viewed with phase-contrast optics (Nikon Plan Apo 60×/1.40 DM objective; Nikon, Melville, NY) and recorded with a Hamamatsu cooled charge-coupled device camera (model C5985; Hamamatsu Photonics, Oak Brook, IL) under control of the Metamorph program (Universal Imaging, West Chester, PA). Images were recorded at 15 frames/min and stored on optical disk (model TQ3038f; Panasonic, Secaucus, NY).

For correlative time lapse-electron microscopy (EM) or time lapse-immunocytochemical studies, cultures were fixed during recording. Fixative was applied by layering ~2.0 ml of the fixative solution on top of the mineral oil. The solution pooled in the center and then dropped through the oil to fix the cultures rapidly and gently.

Fixation, Extraction, and Immunocytochemistry

To reveal localizations of vinculin and phosphotyrosine (Pty) that were confined to adhesion sites, cultures were fixed and extracted simultaneously for 10 min at room temperature with 0.5% Triton X-100 added to a fixative composed of 1% paraformaldehyde in Krebs' buffer (Meiri and Burdick, 1991) with 0.4 M sucrose (n = 30). Fixed cultures were washed three times with each of the following: phosphate-buffered saline (PBS), 0.5 M glycine in PBS, block (1% bovine serum albumin in PBS).

To localize vinculin or Pty labels, fixed and extracted cultures were incubated with either anti-vinculin or anti-Pty monoclonal antibodies (both from Sigma, St. Louis, MO), diluted in block (1:100), either overnight at 4°C or for 2 h at 37°C. Labeled cultures were washed with block and incubated with anti-mouse IgG secondary antibody conjugated to rhodamine (Jackson Immunoresearch, West Grove, PA) and fluorescein-conjugated phalloidin (Molecular Probes, Eugene, OR) to double-labeled for F-actin. After 30 min at

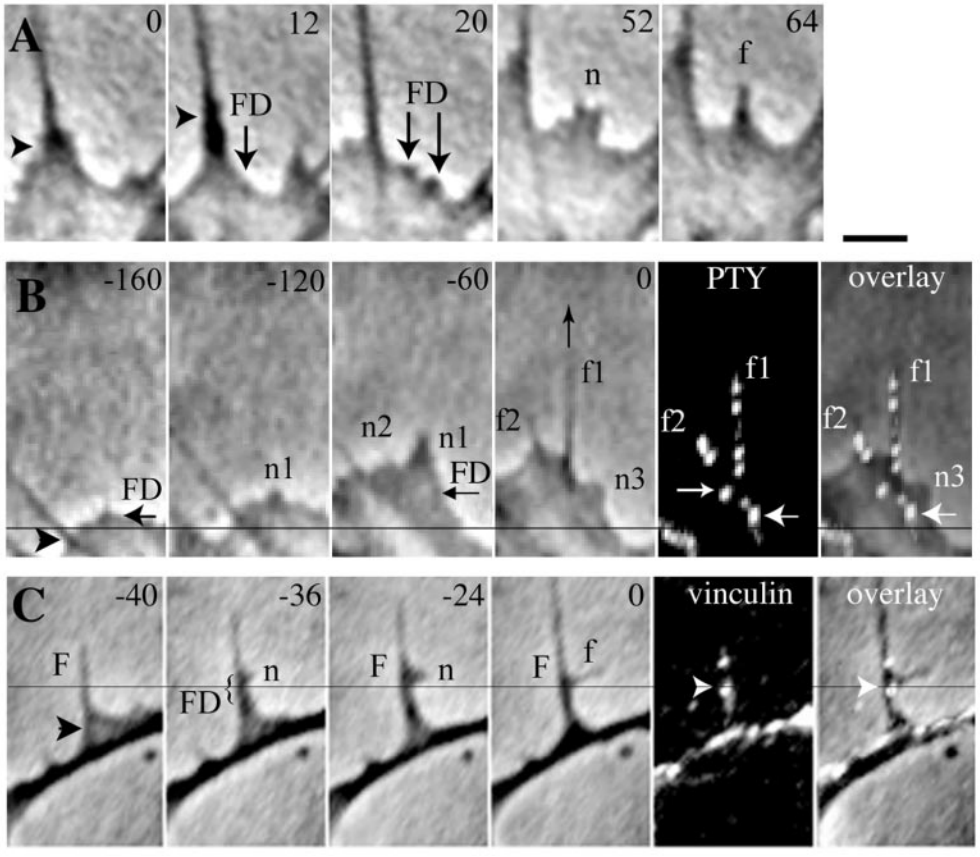

Figure 1. Filopodial initiation exhibits stereotyped features. Figures illustrate the stereotyped characteristics of filopodial initiation as filopodia emerge from veils (A and B) or other filopodia (C). The time elapsed (A) or time before fixation (B and C) is indicated at the top right of each phase frame in seconds. Pty (B) or vinculin (C) label marks adhesion sites present (label and overlay on the frame taken at fixation) and correspond with focal densities (FD) seen in phase. Three features consistently presaged emergence of new filopodia (f): 1) An associated, mature filopodium engorged with cytoplasm, as shown by its increase in diameter and phase density (black arrowheads). 2) FDs developed that correspond to adhesion sites marked by Pty and vinculin labels (B and C). 3) Nubs (n) emerged and transformed into filopodia. Veils ceased extension as nubs emerged. (A) A filopodium bordering an extending veil engorged (arrowheads) then two focal densities formed and resolved into two nubs that fused to form a single filopodium. (B) Pty localized to sites of FDs associated with three initiation phases, at the base of a mature filopodium (f1), the base of a newly emerging filopodium (f2), and the base of an emerging nub (n3). (C) A new filopodium (f) arose from an engorging filopodium (F) at the site of an FD and n. Vinculin labeled the basal adhesion corresponding to the original focal density. Guidelines in B and C reference the first focal density site, FD. Bar, 5 μm

37°C, cultures were washed with block, mounted in Prolong (Molecular Probes) to minimize photobleaching, and viewed with conventional epifluorescence. Images were recorded on optical disks.

Analysis

To identify common features preceding filopodial emergence, we first used a retrospective analysis. Histories of filopodia that emerged successfully were analyzed, both for filopodia extending from veils (n = 100) and from filopodia (n = 100). To test the degree to which the identified features predicted emergence, we then used a prospective analysis. The incidence of filopodial emergence and three features (engorged filopodia, phase densities, and nubs) were assessed in extending veils, where visibility is greatest (n = 254 veils). To analyze immunolocalizations, filopodial initiation sites were identified in recordings and in fluorescent micrographs (n = 45 growth cones). To assess the relation between adhesion sites and filopodial activities, filopodia were classified as extending, shortening, or static just before fixation, and the presence of puncta of label along the base, shaft, or tip was logged (n = 167 filopodia). Regions (tip, shaft, or base) were scored as positive if they had one or more puncta of label. Angles between pairs of newly emergent and engorged filopodia were measured within the first minute of emergence with the use of the Metamorph software package (n = 200). Averages are indicated ± SD. Error bars on graphs show SEM. Significance was tested with the use of paired *t* tests.

EM

Gold, 50-mesh electron microscope grids were coated with 0.6% formvar and lifted onto acid-washed coverslips. Coverslips were affixed over holes drilled through tissue culture dishes and the assembly was coated with poly-ornithine and laminin as described above. Dorsal root ganglion explants were plated into these culture wells in neuron media and motile activities were recorded onto optical discs, as described above. Cells were fixed during recording with 2% glutaraldehyde in PHEM-N buffer (600 mM PIPES, 25 mM HEPES, pH 6.9, 10 mM EGTA, 20 mM $MgCl_2$, and 7.4 mM NaCl, 350 mOsM) for 30 min at room temperature. Some cells were extracted with washes of 0.5% Triton X-100 to better reveal F-actin filaments. Fixed cells were washed in PHEM-N, double distilled-H_2O, post-fixed with aqueous 0.1% osmium tetroxide for 5 min, dehydrated through a graded series of ethanol solutions, stained with ethanolic uranyl acetate, and further dehydrated through hexamethyldisilazane (Electron Microscopy Sciences, Fort Washington, PA). Growth cones were observed intact on the grids with the use of a Phillips CM10 electron microscope operating at 80 kV and photographed onto Kodak 4489 electron image film. Morphologies typical of initiation and emergence were analyzed in 33 recorded and 100 unrecorded growth cones.

To examine whether the focal ring was an authentic structure or an artifact of preparation conditions, different buffers, fixations, extractions, stains, and dehydration protocols were thoroughly assessed. Because ultrastructural entities such as mitochondria and

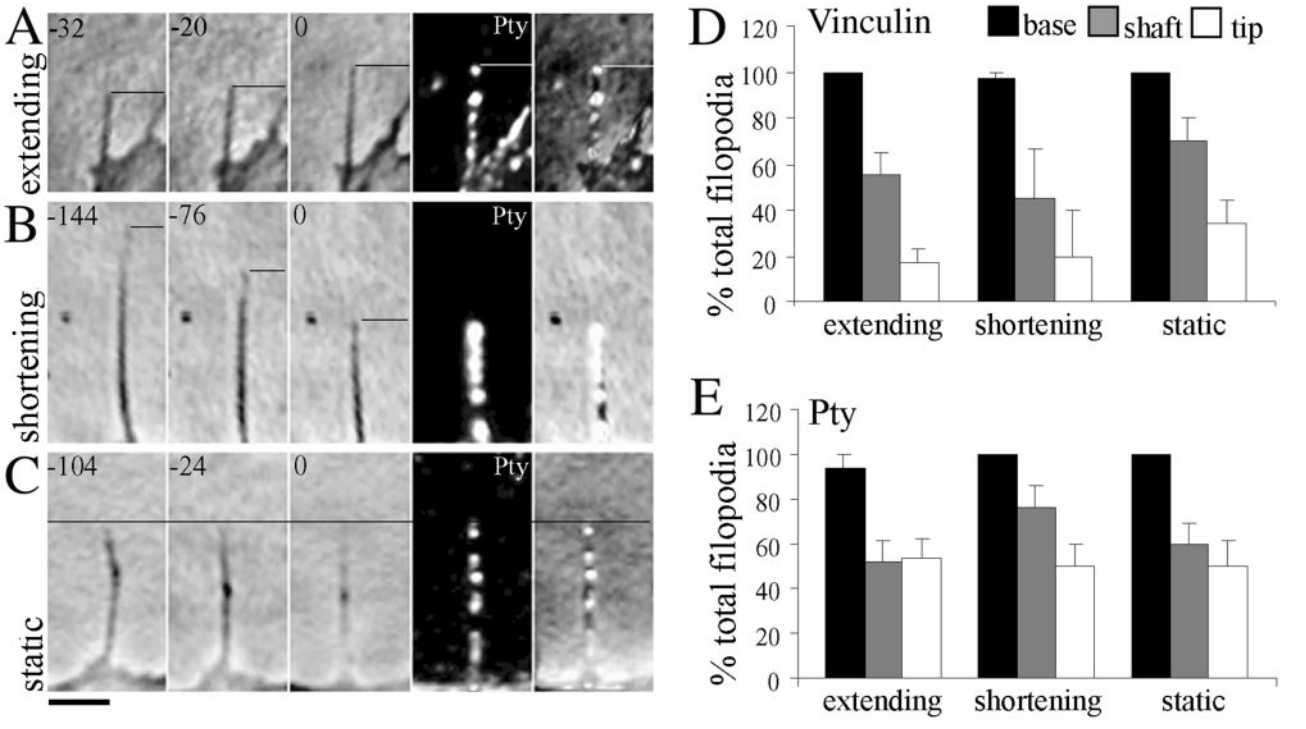

Figure 2. Basal adhesions characterize filopodia regardless of filopodial activities. (A–C) Filopodia exhibiting different motile activities, extending (A), shortening (B), or remaining static (C). Guidelines indicate filopodial tips. The time before fixation is indicated at the top left of each phase frame in seconds. The last two panels in A–C illustrate filopodial adhesions detected by Pty (label and overlay on the frame taken at fixation). (D-C) Adhesions indicated by Pty or vinculin label were classed by filopodial region: base, shaft or tip. Regions were scored as positive if they had at least one punctum of label. Histograms show the percentage of filopodia having adhesions within a region, for each activity. Adhesions failed to accord differentially with filopodial extension, shortening, or stasis. The ubiquity of basal adhesions suggests they play a vital role in all filopodial activities. Bar, 1.0 μm, A–C. D and E: n = 167 filopodia from 20 growth cones. Error bars, SEM

various filaments can vary in appearance with different fixation conditions, we used strict criteria to identify focal rings. In all the preparations, focal rings are defined by their size (120 × 99 nm average maximum and minimum diameters), their oblate donut-shape, their association with radiating filaments, and their position adjacent to the substratum-side of the cell. We particularly screened the bases of all emergent filopodia, because these sites consistently show basal adhesions and associated focal rings after our standard fixation protocols. First, buffer solutions were tested that have been reported to preserve cytoskeletal elements in general, particularly microfilaments, including PBS and 0.1 M sodium cacodylate (used as in Tilney *et al.* 1996a); buffer M, which has been used to preserve actin microfilaments and associated myosin S1 fragment labeling (50 mM imidazole, pH 6.8, 50 mM KCl, 0.5 mM $MgCl_2$, 1.0 mM EGTA, and 0.1 mM EDTA; Svitkina and Verkhovsky, 1995); and a buffer that has been reported to stabilize cytoskeletons (composed of 50 mM imidazole, 50 mM KCl, 0.5 mM $MgCl_2$, 0.1 mM EDTA, and 1 mM EGTA; Svitkina *et al.*, 1997). The best preservation of growth cones in our hands was accomplished with the use of a slight modification of the PHEM buffer (PHEM-N described above) originally constructed to preserve cytoskeletons during detergent extraction (Schliwa and van Blerkom, 1981; Svitkina and Borisy, 1999). Nonetheless, with all buffers tested, focal rings were successfully preserved in the expected sites. Second, the effect of elements known to disrupt or preserve active filaments were assessed directly by including or omitting 2 mg/ml tannic acid, 0.1% osmium tetroxide, 0.01% Triton X-100, 0.01% methanol, or uranyl acetate (Figure 6). For example, tannic acid was used in the primary glutaraldehyde fixative with saponin buffer, because tannate protects actin filaments from fragmentation during osmication (Maupin and Pollard, 1983). In addition, because past studies had used particular regimens to allow reagent penetration or to reveal otherwise hidden structure, protocols were further modified to optimize preservation by manipulating pH, ionic strength, the concentration of Triton X-100 (Tilney *et al.*, 1996a), the concentration of tannic acid that increases the electron density of actin filaments (Maupin and Pollard, 1983), and uranyl acetate to further stain elements (Tilney *et al.*, 1996b). Third, to test the effect of different dehydration schemes, archived EM and high voltage electron microscopy micrographs prepared by K. Tosney (Tosney and Wessells, 1983) were assessed, in which ciliary ganglion growth cones were fixed under a variety of fixation conditions and then, rather than being dehydrated through hexamethyldisilazane, were critical point dried. All the regimens used, except for those very thorough extractions that removed everything but some actin cytoskeleton, revealed focal rings and associated actin filaments at filopodial bases.

EM-Immunocytochemistry

Cultures were fixed with 2% paraformaldehyde/0.05% glutaraldehyde in buffer M (50 mM imidazole, pH 6.8, 50 mM KCl, 0.5 mM $MgCl_2$, 1.0 mM EGTA, and 0.1 mM EDTA; Svitkina *et al.* 1997) for 20 min at room temperature. Fixative with the use of PHEM-N buffer gave identical results. Fixed cultures were washed with buffer M (described above), permeabilized by rapidly rinsing with 0.05% Triton X-100 in buffer M, and then washed several times with buffer M followed by PBS. Permeabilized cultures were incubated for 10 min with 1% bovine serum albumin (block) to inhibit nonspecific

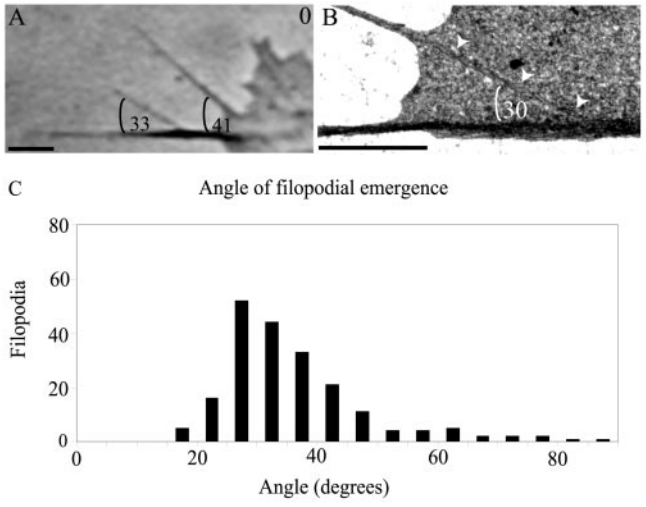

Figure 3. Filopodia emerge at stereotyped angles. When examined during their emergence, new filopodia are oriented at a stereotyped angle with regard to the adjacent, engorged filopodium. Emerging filopodia were monitored with time lapse, and the angles of their emergence measured relative to the engorged filopodium. (A) Phase image shows two filopodia that intersect a filopodium that is engorged, as shown by its larger diameter and greater phase density. The newer filopodium intersects at 33 degrees, whereas the older filopodium has pivoted and intersects at 41 degrees. (B) Filopodium at top had emerged within a minute before fixation and processing for EM. The engorged filopodium at bottom exhibits higher electron density. The internal filament bundle of the newly emergent filopodium (white arrowheads) intersects the engorged filopodium at a 30 degree angle. (C) Angles of emergence were measured, relative to the adjacent engorged filopodium, from time lapse frames taken within 1 min after nub formation. Values are binned in 5 degree increments. n = 200; mean, 36.2 ± 12.3. Bars, A and B, 5 μm.

binding, followed by rabbit anti-actin antisera (Sigma) and 10-nm gold particles conjugated to protein A (Sigma), both in block. Labeled cultures were postfixed with 2% glutaraldehyde in PBS, stained with uranyl acetate, dehydrated, and observed as described above.

RESULTS

In the growth cones we examined, filopodia emerged from four distinct sites: 1) the leading edge of extending veils (Veils are active lamellar protrusions that extend between filopodia in growth cones.); 2) the shafts of preexisting filopodia; 3) less seldom, from internal sites; and 4) rarely, from the neurite. Veils afford the greatest visibility due to their simplicity and optical thinness, and so filopodial initiation in veils received the most detailed analysis. To qualify for analysis, the veil had to have protruded at least 2 μm from the growth cone margin.

Motile Histories Reveal Events Presaging Filopodial Initiation

To identify events that presage filopodial emergence, we first used a retrospective analysis. Filopodia were selected that had emerged from veils (n = 100) or from filopodia (n = 100) and their history was analyzed, to ask what most (80–100%) had in common. As detailed below, emergence was consistently presaged by development of a focal phase density, engorgement of an associated mature filopodium, and protrusion of a convex "nub" that subsequently transformed into a filopodium. The degree to which these events are predictive was then tested with the use of a prospective analysis of events in extending veils (Table 1). This analysis shows that, when only one or two of these events was detected, filopodia emerged 0–38% of the time, whereas when all three events were detected, filopodia emerged 86% of the time. The three events described below are thus robustly associated with filopodial initiation.

Emergence Is Preceded by Development of a Focal Phase Density A focal phase density regularly developed before filopodia emerged from either a veil or a preexisting filopodium (Figure 1). When examined retrospectively, a small, phase dense spot had always formed at the leading margin of the veil (100/100) or along the parental filopodium's shaft (100/100). In prospective analysis, when phase densities developed, filopodia commonly emerged at that site (85% or 179/211). In contrast, when focal densities were not detected, few filopodia emerged (16% or 7/43). These results support the importance of focal densities. However, focal densities by themselves appear insufficient for initiation. Even when phase densities were present, filopodia failed to emerge when both other events were absent (0/3), and seldom emerged if even one other event was absent (14%: engorgement absent 3/11; nub absent, 0/10). Focal density formation is likely to be a vital control point for initiation, but one that is subject to regulation.

Even when the veil margin advanced, these focal phase densities remained stationary with regard to the substratum, suggesting that they mark an adhesion site. To test further for adhesion, immunolocalization of two adhesion markers, vinculin and Pty, was examined with the use of conditions that preserve label selectively at adhesion sites. Focal densities labeled consistently, whether they were associated with the veil margin (6/6 vinculin; 6/6 PTY) or with the base of nubs (6/6 vinculin; 6/6 Pty; Figure 1, B and C). Moreover, the phase densities and immunolocalizations persisted. For instance, the stable bases of filopodia consistently labeled (vinculin, 99%, 101/102; Pty, 97%, 77/79).

Based on stability with regard to the substratum and localizations of vinculin and Pty, filopodial initiation is typically preceded by the development of an early and persistent substratum adhesion. Because these adhesions are an elementary step in filopodial initiation and because they anchor the bases of the ensuing filopodia, we consider them to be a distinct adhesion and refer to them as "basal adhesions."

Basal adhesions were ubiquitous among filopodia, regardless of filopodial activities. Filopodial adhesions detected by vinculin or Pty label were assessed along different filopodial regions (base, shaft, tip) in filopodia that were extending, shortening, or static. Adhesions along shaft or tip may or may not be present during these activities, but basal adhesions characterized nearly all filopodia (Figure 2). Even when the tip and shaft were moving laterally, filopodia retained the basal adhesion, even though they usually lacked label at any other site (also see Argiro *et al.*, 1985; Bray

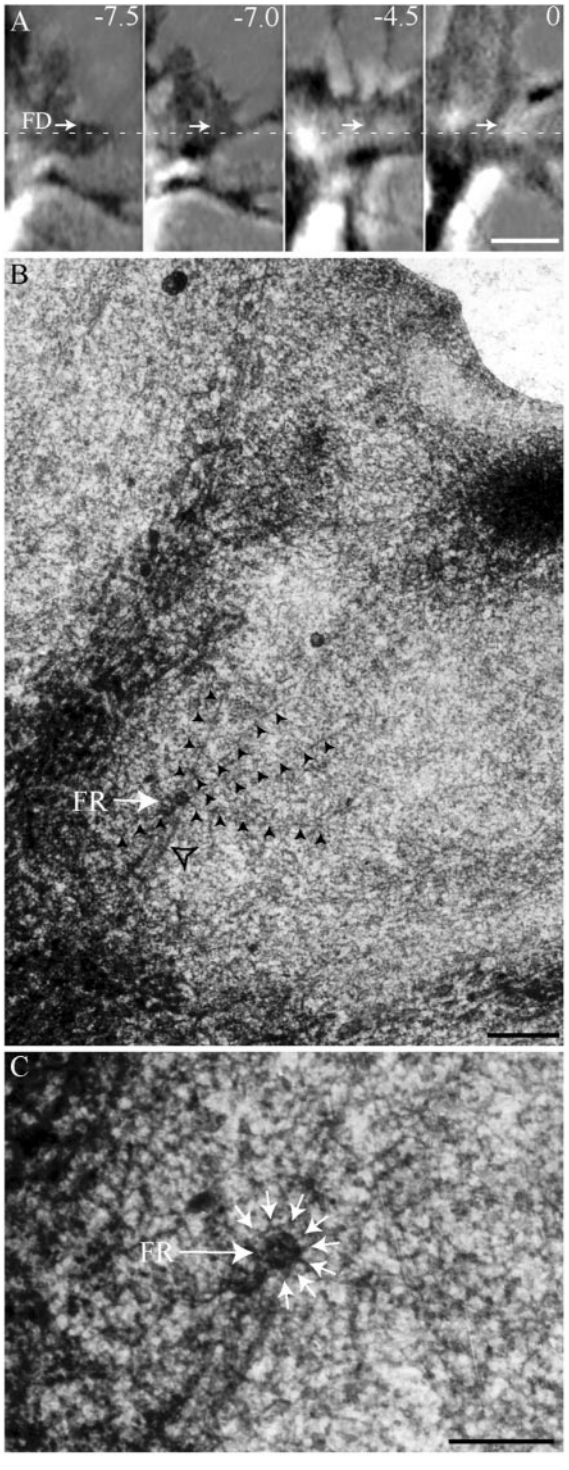

Figure 4. Focal densities persist in place and display focal rings. (A) Growth cone margin was monitored with the use of optical recordings during filopodial emergence. The time before fixation is indicated at the top right of each frame in minutes. A focal density (FD, arrows) was associated with the development of a nub that formed a filopodium. As the growth cone advanced, this focal density persisted in the same site (arrows) relative to the substratum, as indicated by the white guideline. This site was then examined in EM, with the use of landmarks such as phase-dense streaks that indicate filament bundles. (B) Landmarks can be identified in an electron micrograph of the same region viewed at relatively low magnification (compare with time 0 in A). At the site of the focal density lies a focal ring (FR). The focal ring radiates long filaments (e.g., black arrowheads). An apparent microtubule ends near the focal ring (open arrowhead). (C) Higher magnification reveals the typical donut-shaped structure of a mature focal ring. It also shows that filaments intersect this focal ring in an apparently repetitive pattern, indicated by the 30 degree placement of arrowheads. Bars, A, 1 μm; B, 500 nm; C, 250 nm.

and Chapman, 1985). Their ubiquity suggests that basal adhesions are important to a variety of filopodial activities.

Emergence Is Preceded by Cytoplasmic Influx Filopodial emergence was consistently presaged by an influx of cytoplasm into an associated mature filopodium, a process termed engorgement. Engorgement characterized all successfully emergent filopodia in the retrospective analysis, whether they emerged from veils (100/100) or from filopodia (100/100). Engorgement was also associated with the vast majority of filopodia emerging from veils in the prospective analysis (98% or 183/186; Table 1). Engorgement was detected by a progressive increase in the phase density and thickness of the filopodium, which progressed from proximal to distal (Figure 1). The phase dense material seldom filled the entire filopodium, and the increased density and thickness were often transient, unlike the persistent phase density that characterizes the basal adhesion site. The influx of cytoplasm usually preceded or was concurrent with focal density formation.

Engorgement appears to be important but insufficient by itself to initiate filopodia. When engorgement was seen, filopodia failed to emerge when both other events were absent (0/11). Despite the presence of engorgement, filopodia seldom emerged if even one other event was absent (18%: phase density absent, 7/28; nub absent, 0/10). On the other hand, a single engorging filopodium appears to suffice. Initiation rates were the same regardless of whether only one, or both supporting filopodia engorged. These results suggest that initiation requires materials that are transported down a filopodial shaft.

Emergence Is Preceded by Protrusion of a Nub Nubs are convex projections with wide bases; they are transient, with lifetimes typically $<$1 min (Figure 1). As a nub transforms into a filopodium, it narrows to form a cylindrical shaft, and it lengthens. In veils, the nascent shaft is delineated by the retreat of the veil margin as well as by elongation. Nub morphogenesis can be complex. Several nubs could develop within the same veil and generate several filopodia, or several nubs could merge and generate a single filopodium. Nub productivity also varied. Filopodia that emerged from nubs differed in sizes and lifetimes, ranging from small transient filopodia lasting seconds to large persistent filopodia lasting minutes. Nub size tended to predict success; the larger the nub, the larger and more persistent the filopodium.

Nubs characterized successful filopodial initiation, both in retrospective (91% or 182/200) and prospective (81% or 186/229) analyses. Although a few nubs were detected that did subsequently regress, nubs were probably under-

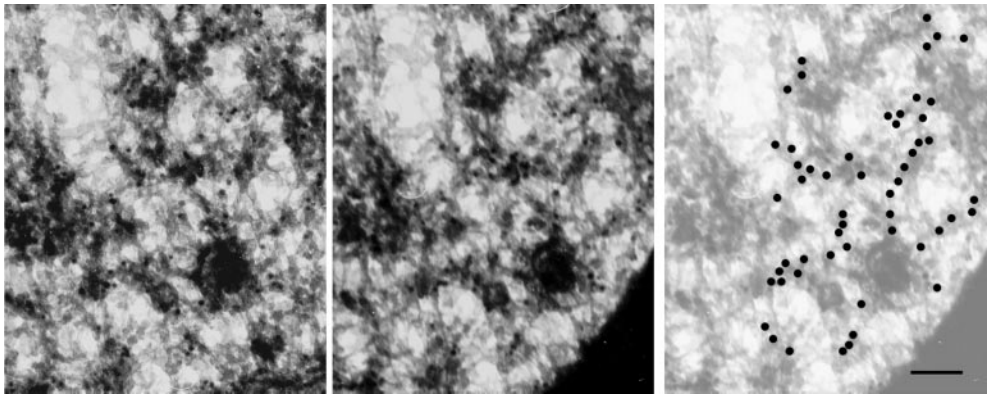

Figure 5. Focal rings radiate actin filaments. In immuno-EM, filaments that radiate from focal rings label for actin. Left and center; stereo pair. Right, low contrast image, with gold particles highlighted by black dots. Rabbit anti-actin primary antibody, secondary antibody conjugated to 10-nm gold. Bar, 100 nm.

counted, because any that were particularly short lived or that developed out of the focal plane or behind a mature filopodium would have been missed. As with engorgement and phase densities, nubs appear important but insufficient for filopodial initiation. Nubs could form when both engorgement and densities were absent. However, the three that did so all failed to generate filopodia. When a nub was present, only 28% matured into a filopodium when one other event was absent (engorgement absent, 3/8; phase density absent, 7/28).

Nub emergence also correlated with changes in veil extension. As nubs emerged from veil margins, the veil invariably stopped extending, regardless of whether the nub spawned a filopodium or not (100/100; Figure 1). Extension appears to be converted from a lamellar to a filopodial mode.

Emerging Filopodia Often Associate with Preexisting Filopodia New filopodia tended to emerge at a common angle with regard to the engorged filopodium (Figure 3). During their emergence, filopodia were most commonly oriented at an angle ranging from 20 to 60 degrees (with a peak near 30 degrees and a long tail; mean, 36.2 ± 12.3, n = 200). This initial congruency was transient, because filopodia later moved laterally and assumed various angles. In addition, when the shaft of a new filopodium had been revealed by extensive veil regression, it appeared to intersect a more mature filopodium (100/100). These observations suggest an interaction between emergent and adjacent engorged filopodia that depends on defined architectural rules of association among cytoskeletal elements.

Correlative Whole-Mount EM Reveals "Focal Rings" at Basal Adhesion Sites When focal phase densities were examined with the use of correlative time lapse-electron microscopy, the sites always contained a novel structure, a focal ring (Figure 4; n = 181/181). In time lapse, focal phase densities persisted, in accord with a function in adhesion. They formed at veil margins and then remained in place relative to the substratum, despite advance of the growth cone (Figure 4A). When these persistent sites were examined in the same recorded growth cones with the use of EM, a focal ring and radiating filaments were clearly visible (Figure 4, B and C). Focal rings are thus a consistent feature of basal adhesion sites.

Focal rings displayed stereotyped morphologies and positions (Figures 4C and 5). Focal rings were shaped like oblate donuts with maximum (120 ± 27 nm) and minimum (99 ± 23 nm) diameters differing significantly ($p < 0.0001$; n = 102 rings in 79 growth cones). They contained an apparently hollow core that could appear electron lucent (Figure 4C) or electron dense (Figure 5). When viewed in stereo, the focal rings lay on the substratum side of the cell (Figure 5). Their coincidence with stable adhesion sites, their ventral position, and their resistance to detergent extraction (Figure 6, B, D, and E) all suggest that focal rings are associated with development of a stable adhesion.

Focal rings had characteristic relations with filaments. Note that in discussing filament relationships, *terminate* and *radiate* describe filament architecture without implying filament polarity. *Filament* refers to individual filaments ~6 nm in diameter (F-actin microfilaments). *Bundle* refers to more than one filament closely opposed.

Filaments radiating from focal rings are actin filaments. In immuno-EM, the focal ring itself very seldom showed gold particles indicating F-actin label, but filaments associated with the focal ring consistently labeled for F-actin (Figure 5; n = 50/50 rings). The filaments often appeared to radiate from spokes within the focal ring, and the spokes likewise did not label for F-actin. Some spokes were unassociated with a radiating filament, and in the few cases in which spokes were undetectable, filaments terminated directly on the focal ring's outer margin. Generally, focal rings displayed 3–12 spokes, often at 30 degree increments (Figure 4C), in curiously similar correspondence with the angle of new filopodial emergence (Figure 3).

Filaments radiating from focal rings sometimes extended blindly into the veil but generally terminated at nub tips, on other focal rings or on filament bundles. When these filaments contacted bundles, they generally did so at a common angle (60 ± 13 degrees; n = 23). The angle of intersection was similar when a filament could be traced to intersect on an individual filament within a bundle (56 ± 16 degrees; n = 10). Most filaments interconnecting focal rings and other structures were gently curved or straight as although under tension, whereas those that failed to terminate obviously on another structure were usually kinked, sinuous, or meandering. In addition, microtubules (filaments 23 ± 2.4 nm in

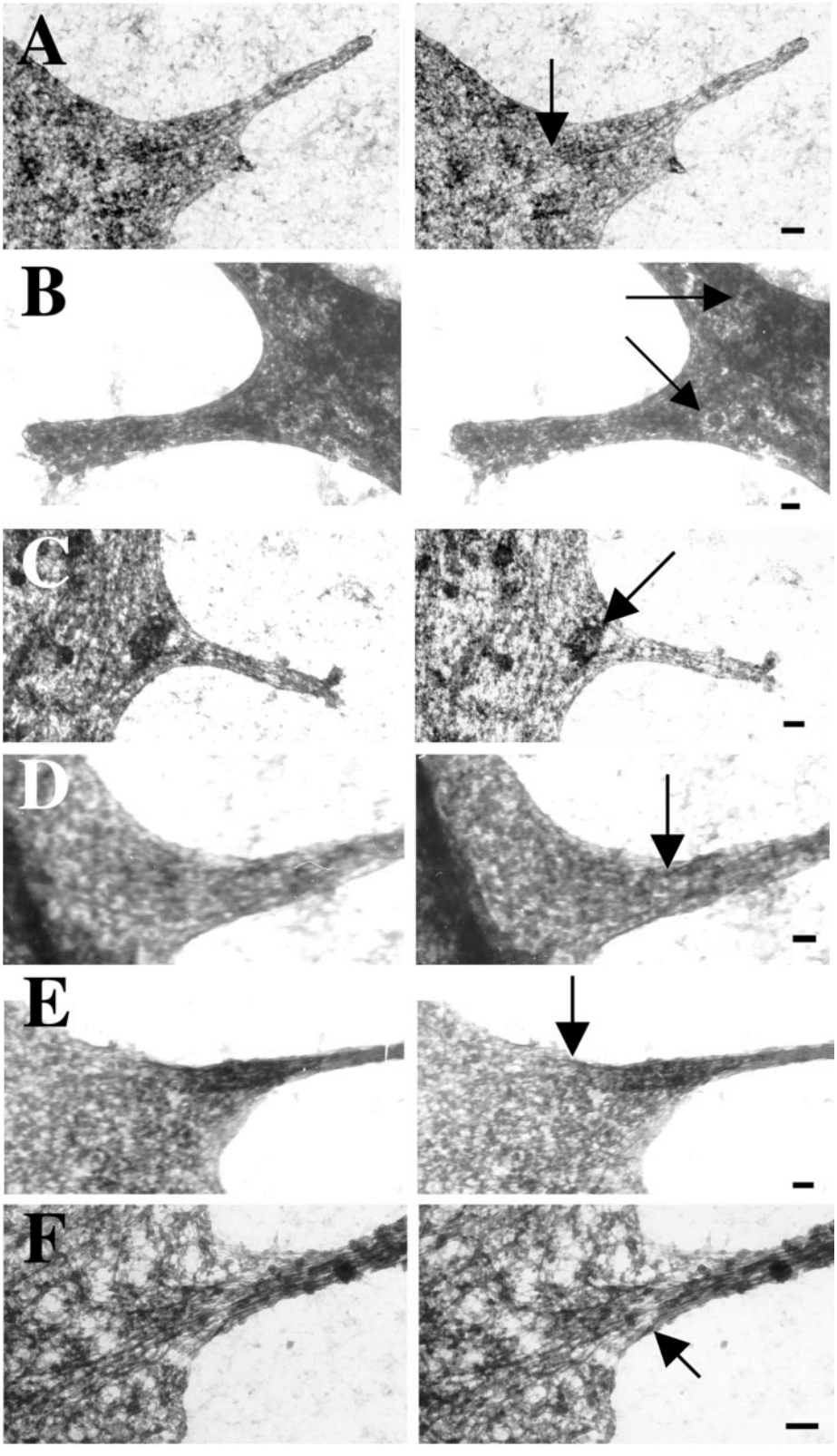

Figure 6. Focal rings are detected at filopodial bases after a variety of fixation regimens. To examine whether the focal ring was an authentic structure or an artifact of preparation conditions, different buffers, fixations, extractions, stains, and dehydration protocols were thoroughly assessed. In all the preparations, focal rings are defined by strict criteria based on their size (120 × 99 nm average maximum and minimum diameters), their oblate donut-shape, their association with radiating filaments, and their position adjacent to the substratum-side of the cell, as shown in stereo pairs. In fixation trials, we focused on basal adhesion sites at the bases of emergent filopodia. Examples shown here were fixed with 1.5% glutaraldehyde in PHEM buffer and stained with uranyl acetate. Arrows indicate focal rings at filopodial bases. (A–C) With osmium tetroxide. (D–F) Without osmium tetroxide. (A, B, and D) With tannic acid. (B and D) With Triton X-100 extraction. (E) With methanol extraction. Bars, 100 nm.

diameter; n = 6) sometimes extended between focal rings and the central growth cone (Figure 4B).

Focal rings are unlikely to be an artifact of the fixation regimen, because they were detected at basal adhesion sites regardless of fixation regimen (Figure 6). Regimens that altered fixation buffers, or the presence or absence of osmium, tannic acid, and uranyl acetate, or that lightly extracted with the use of Triton X-100 or methanol, still revealed typical donut-shaped structures of the correct dimensions at a predicted site, the bases of filopodia. In addition, our standard dehydration used hexamethyldisilazane, but, dehydration with the use of critical point drying also revealed rings at filopodial bases (Tosney, unpublished results; Tosney and Wessells, 1983, e.g., stereo Figures 2 and 8).

Focal rings were detected at adhesion sites associated with stabilization. They were particularly obvious at the bases of filopodia (Figure 6), regardless of whether the filopodium arose from a veil (Figure 7, A–C), another filopodium (Figure 7D), or a neurite (Figure 7E). They were also detectable at the bases of filopodia-like projections in Schwann cells (our unpublished results). Focal rings were also seen at adhesion sites typifying stably retracted veils (defined in time lapse as veils that had retracted and then remained unmoving for at least a minute before fixation). These margins typically had one or more subjacent focal rings with radiating filaments that paralleled the veil margin and intersected filament bundles in adjacent filopodia (Figure 7F; n = 180/180, Table 2). These focal rings and filaments may demark the proximal limit of veil retraction and help stabilize the margin. In addition, when observed in partially extracted growth cones, focal rings were particularly prominent near the internal termination of filament bundles (Figure 8). At these sites, they often appeared to be linked by "slings" of filaments, as although playing a vital role in cytoskeletal linkage and stabilization.

The other common type of projection seen on growth cones typically lacked focal rings at its adhesion site. Triangular projections differ from nubs and filopodia because they end in a sharp point, rather than a rounded arc (hence, their designation as triangular). They are invariably adherent at their tips, unlike nubs and filopodia, which are adherent at their bases. Also in contrast to nubs and filopodia, triangular projections form as the margin retracts away from small adhesion sites, rather than through active protrusion. Triangular projections consistently lacked focal rings (Figure 9; 0/100 had focal rings, Table 2). These observations indicate that structures associated with filopodial emergence can be clearly distinguished from other surface projections, and that other projections lack the focal rings characteristic of filopodial emergence and stability.

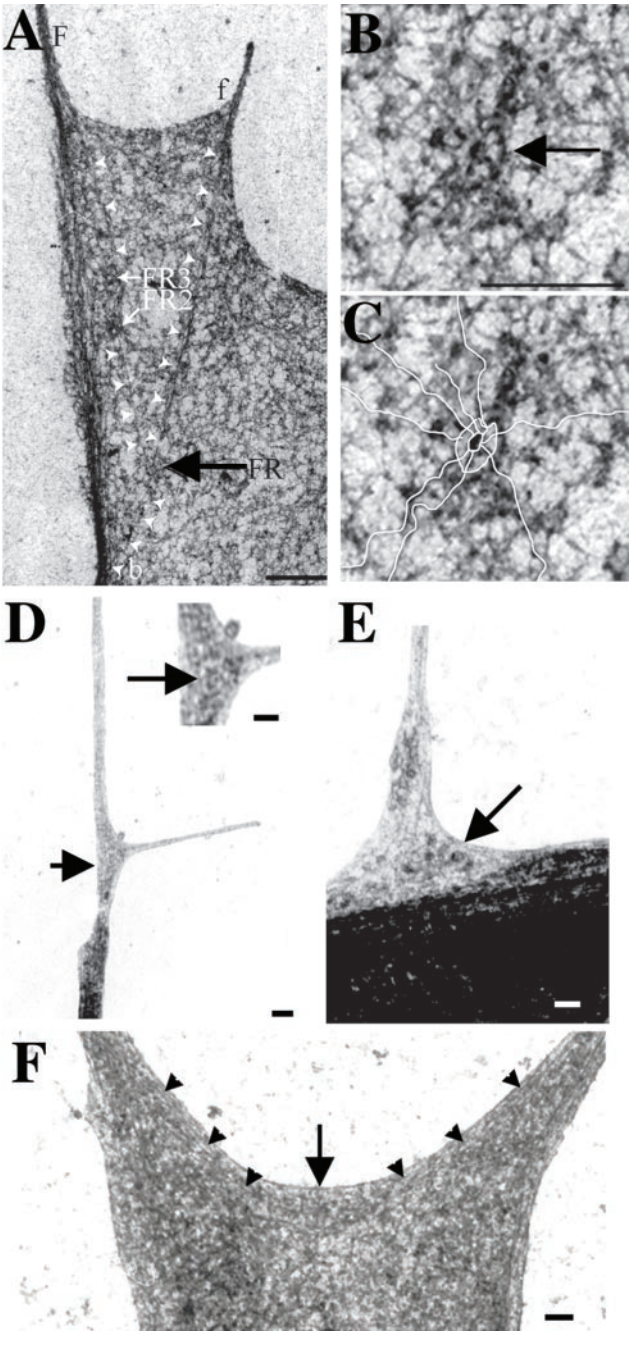

Figure 7. Focal rings characterize stable sites and show a stereotyped morphology and filament associations. Motile activities were monitored in time lapse, and the distribution of focal rings (arrows) was examined in EM. (A) Focal rings lie at the origin of filamentous bundles (FR, arrow) and along filaments (FR 2, 3). (B and C) Typical focal ring displays an oblate donut-shape with periodic spokes that often connect with the radiating filaments, highlighted in C. Focal rings also characterized bases of filopodia that originated from other filopodia (D, arrow and inset) or from neurites (E). (F) This veil had retracted and stabilized just before fixation. Its margin was concave and was underlain by long, aligned filaments (arrowheads) that interconnected filaments in adjacent filopodia with a focal ring (arrow). Bars, A–C, 250 nm; D–F, 100 nm.

Correlative Analysis Reveals Focal Ring Assembly and Relations at Initiation Sites

Correlated time lapse-EM also documented focal ring development and revealed characteristics of initiation phases. The first two phases were documented by recording veils that were fixed as phase densities developed at their margin (Figure 10); subsequent phases were documented by recording veils that were fixed as nubs appeared and transformed into filopodia (Figure 11). For each phase, the same areas in the same growth cones were then examined with the use of

Table 2. Incidence of diagnostic morphologies in recorded and unrecorded growth cones

	Recorded n = 33		Unrecorded n = 100		Totals	
	No.	% of class	No.	% of class	No.	% of class
(A) Initiation phases in extending veils						
Initial adhesion	45	30	119	29	164	29
Focal ring genesis	13	9	66	16	79	12
Nub formation	48	32	122	30	170	30
Bundling	43	29	102	25	145	26
(B) Filopodia						
Newly emergent	32	11	103	11	135	11
Intersecting	49	18	196	22	245	21
Mature	190	68	555	62	745	63
Retracting	8	3	46	5	54	5
		n		n		Totals
(C) Veils without initiations						
Extending veil		21		55		76
Retracted veil		180		549		729
(D) Adherent triangular projection		30		70		100

Electron micrographs of 33 recorded and 100 additional growth cones were examined. The incidence of morphologies typical of different activities was tabulated. The percentage of each morphology within classes A (extending veils) and B (filopodia) was calculated. (A) Initiation phases, in temporal order. At the initial adhesion phase, the margin was locally tethered to the substrate and this adhesion site showed marginal electron densities, as in Figure 10D. At the focal ring genesis phase, the margin was not adherent and an adherent focal ring had developed at the margin, as in Figure 10E. At the nub formation phase, a nub had protruded and at least one basal ring was apparent, as in Figure 11, A–C. At the bundling phase, the nub had formed a more cylindrical form and filaments were partially bundled with the axial filament, which terminated in a focal ring, as in Figure 11D. (B) Filopodia, listed in order of maturity. Newly emergent filopodia were short and had one or two rings basally and little proximal shaft, as in Figure 6. In intersecting filopodia, the proximal shaft intersected one or more rings and terminated on the shaft of a more mature filopodia (Figures 3B and 7A). In mature filopodia, the shaft intersected focal rings and extended far proximally (Figure 8). Filopodia that were kinked or irregular were considered to be retracting. Their shafts were often shortened and splayed. (C) Veils without initiating filopodia. Extending veils had convex or straight margins. Those without initiations lacked electron densities, focal rings, or long submarginal filaments. Retracted veils had concave margins underlain by long, lateral filaments that extended between a focal ring and adjacent filopodial bundles (Figure 7F). (D) Adherent triangular projections. These structures resembled nubs in being small projections, but they were adherent at their tips, were not cylindrical, lacked both marginal electron densities and focal rings, and formed as the margin withdrew, rather than by active extension (Figure 9) (n = 649 sites in 133 growth cones).

EM. The diagnostic morphologies for each phase were so distinctive that they could be relied upon to infer the phase of initiation even in unrecorded growth cones (Table 2). The incidence of each initiation phase per growth cone varied, as expected given the dynamic variation among growth cones, but at any one time each growth cone averaged 4.2 ± 2.1 sites at some phase of initiation (n = 649 sites).

For clarity, we distinguish three filament classes that develop during initiation, based on different terminations. Radial filaments, those filaments with one termination on a focal ring, are organized into two classes: *axial filaments*, which terminated at the plasma membrane, and *lateral filaments*, which terminated on filament bundles, other focal rings, or within the veil milieu. A third class, *nub filaments*, extended from nub tips but failed to terminate on a focal ring.

During the *initial adhesion phase* (site FD1, Figure 10) the veil had a convex or straight margin typical of veils that were actively extending, and most of the margin was clearly free of the substratum. However, at the initiation site itself, the margin always contacted the substratum locally via small, evidently membranous, tethers (164/164), directly suggesting it was adherent. This portion of the margin regularly contained electron densities. Typically, a few long lateral filaments extended from the site to terminate on filament bundles in adjacent filopodia or on more proximal focal rings.

During the *focal ring genesis phase* (site FD2, Figure 10), the margin at the initiation site had begun to protrude away from the basal adhesion site, which displayed a nascent focal ring (n = 79/79). The margin was seldom directly tethered to the substratum, and it often clearly protruded upward. In stereo pairs a focal ring always appeared close to the substratum side of the membrane and when an uplifted margin allowed close examination, tethers could be seen that evidently connected the focal ring site itself with the substratum (Figure 11B, site a). A few (2–6) lateral filaments commonly radiated from this focal ring to filament bundles and other focal rings, and in some cases, despite the proximity of focal ring and margin, an axial filament was detectable. The low proportion of this phase present per growth cone at any one time (14%; Table 2) suggests that focal ring genesis is rapid, although the proportion cannot reflect phase duration directly because some phases may regress without successful issue.

During the *nub formation phase*, typical filament associations had emerged and the veil margin had ceased to extend and begun to relax inward, forming a concave outline that

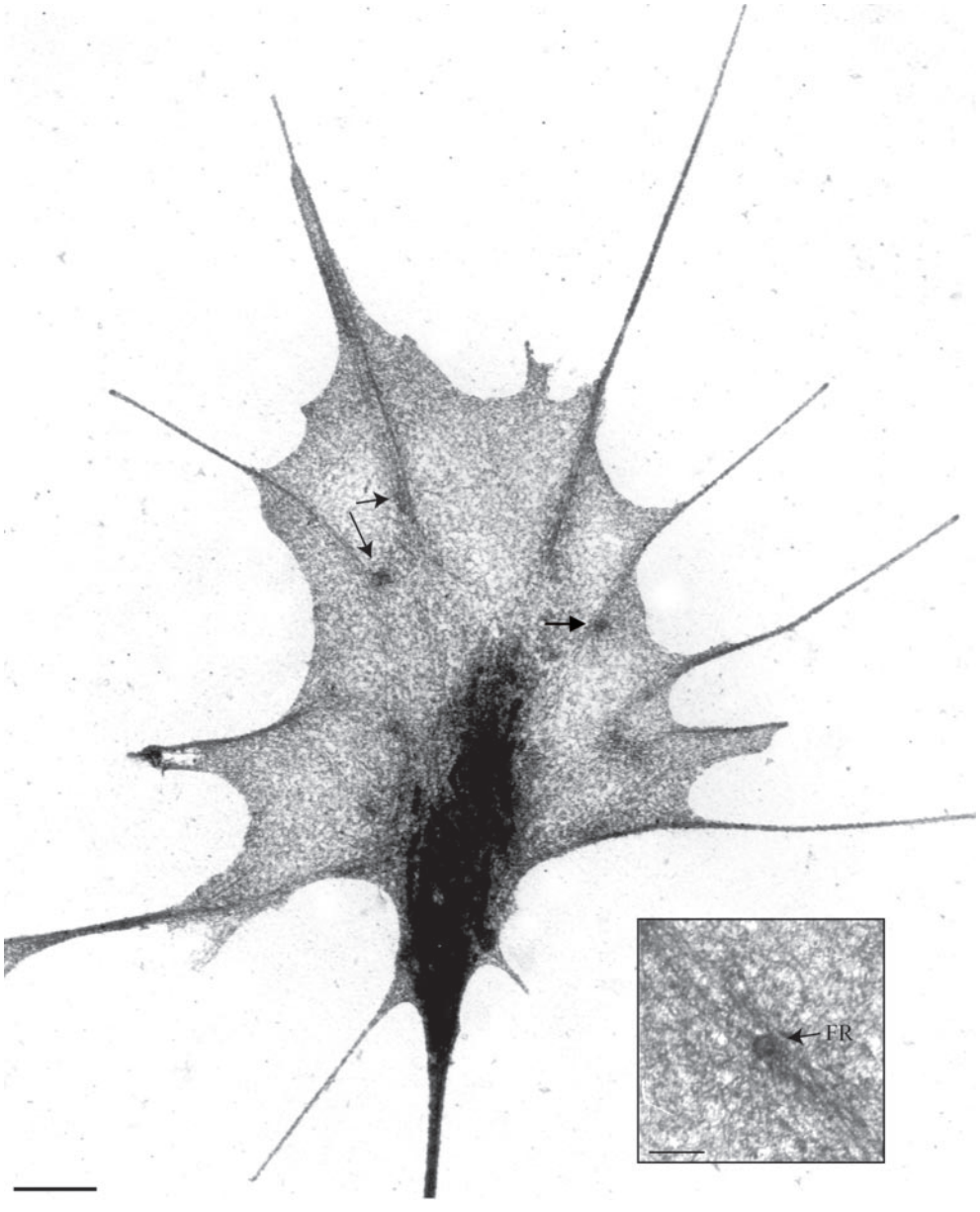

Figure 8. Focal rings characterize basal adhesions of mature, stabile filopodia. Low-magnification EM of this extracted growth cone reveals focal rings (e.g., arrows and insert) at the bases of filopodial filament bundles. Filaments radiating from these focal rings often intertwine, forming slings between filopodial bases. Bars, 1 μm; 200 nm (insert).

would ultimately delineate the filopodial shaft (Figure 11, A–C). One or more focal rings characterized the prospective base of all emerging nubs (n = 170/170), and when observed in stereo the focal rings were adjacent to and roughly parallel with the substratum. When focal rings were still close to the margin, tethers could commonly be seen that appeared to interconnect the undersurface of the veil with the substratum, as although emanating from the focal ring site (Figure 11, A and B). Generally, one or two axial filaments connected the focal ring and nub tip, and a few nub filaments splayed proximally.

During the *bundling* phase, the nub assumed a more cylindrical shape as the margin retracted further, and the nub and axial filaments appeared to bundle together, from distal to proximal, as although oriented by the axial filament (Figure 11D). Focal rings were invariably seen at the base of the nub (n = 145/145). Generally, the initial numbers of filaments within nubs and nascent filopodia was small and more actin filaments appeared after the filopodium achieved cylindrical form and began to elongate.

Engorgement was also obvious. During initiation, an adjacent engorged filopodium consistently displayed high electron density along its shaft (right filopodium, Figure 10; bottom filopodium, Figure 3B). The high density was usually obvious even during the first phase, but often persisted and was detectable even later, after a new filopodium had emerged. Surprisingly, in many cases the engorged regions lacked membranous organelles and simply contained more electron dense accumulations, consistent with the distal

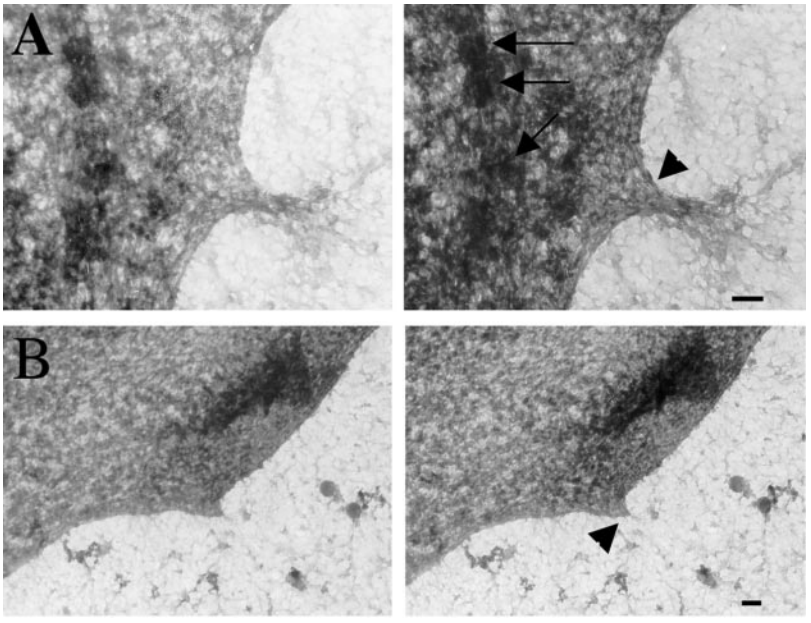

Figure 9. Specializations characteristic of filopodial initiation do not arise at other adhesion sites. Projections that superficially resemble nubs can form by a process that does not involve active extension. Such triangular projections form when the margin adheres and then withdraws from the adhesion site. When examined in EM, these triangular projections lack the rounded tip morphology and marginal specialization typical of nubs, and consistently lack focal rings at their bases, as shown here in stereo pairs. (A) Triangular projection (arrowhead) is adherent at its tip but lacks marginal specializations or a distinct focal ring, despite the association of focal rings (arrows) with nearby filament bundles emanating from a filopodium. Note also that the focal rings lie below the bundled filaments, adjacent to the substratum side. (B) Triangular projection at the edge of an extending lamella lacks marginal specializations or a basal focal ring. Bars, 100 nm.

movement of regulatory and structural proteins or molecular complexes.

DISCUSSION

This study documented events and structures underlying filopodial initiation. Motile histories revealed three features that consistently forecast filopodial emergence (engorgement, focal density development, and nub protrusion), thereby permitting putative initiation sites to be identified and examined in the same cells to reveal adhesive and ultrastructural specializations. This correlative analysis revealed that focal phase densities mark basal adhesion sites that develop a focal ring, a putative actin organizer.

The results support a model in which focal rings and their radiating filaments play a fundamental role in filopodial initiation, development, and stability (Figure 12). The model focuses on initiation during veil extension where events are most easily distinguished and tested, but it applies to filopodia initiation from other sites as well. The model posits a stereotyped sequence of events in which three processes are essential to filopodial initiation: 1) engorgement; 2) development of basal adhesions and focal rings; and 3) nucleation, elongation, and bundling of filaments. In this model, focal rings play a vital role in initiating and stabilizing filopodia. They are posited to nucleate actin filaments, and to anchor the actin filaments at basal adhesion sites, thereby facilitating tension development and filopodial emergence. Their "axial" filaments connect focal rings to nub tips and orient bundling of "nub" filaments that nucleated at the nub tip, thereby assuring that the bundle intersects a basal adhesion. Their "lateral" filaments interconnect focal rings and filament bundles, thereby helping stabilize both lamellar margins and filopodia.

Engorgement

In this model, before a filopodium emerges, engorgement supplies essential materials for transforming actin dynamics from a lamellar to a filopodial mode, and for developing specialized, "basal" adhesions (Figure 12A). Engorgement detected in phase or electron microscopy was consistently associated with filopodial emergence. Previously, engorgement in growth cones has been invoked as important in selecting a broad area that will preferentially advance (Goldberg and Burmeister, 1986). Engorgement is also known to be susceptible to control by guidance cues, because contact with specific cellular cues can steer growth cones by specifically stimulating the contacting filopodia to engorge (O'Connor *et al.*, 1990; Smith, 1994; Steketee and Tosney, 1999). In at least one system, induced engorgement is accompanied by increased filopodial initiation (Steketee and Tosney, 1999). However, a specific relation between engorgement and filopodial initiation was previously unrecognized.

Basal Adhesions

Basal adhesions are proposed to be specialized adhesion sites that arise by a process requiring engorgement, and that organize the molecular effectors necessary for constructing and maintaining a filopodium (Figure 12B). That they are indeed adhesion sites was shown by three criteria: their stability relative to the substratum when viewed as focal phase densities in time lapse, their display of two adhesion-dependent localizations (vinculin and Pty), and their display of membrane tethers to the substratum. Various similar adhesions have been inferred previously, but such studies did not directly examine relations of adhesions to filopodial initiation (e.g., at birefringent spots in *Aplysia* growth cones, Katoh *et al.*, 1999; close contacts in keratocytes, Lee and Jacobson, 1997; and possibly subsets of "point contacts" in growth cones, Renaudin *et al.*, 1999).

Basal adhesions appear to be specialized, because not every adhesion supports filopodial initiation. Multiple adhesions can exist along filopodial shafts (Figure 2; Arregui *et al.*, 1994; Gomez and Letourneau, 1994), but most generally

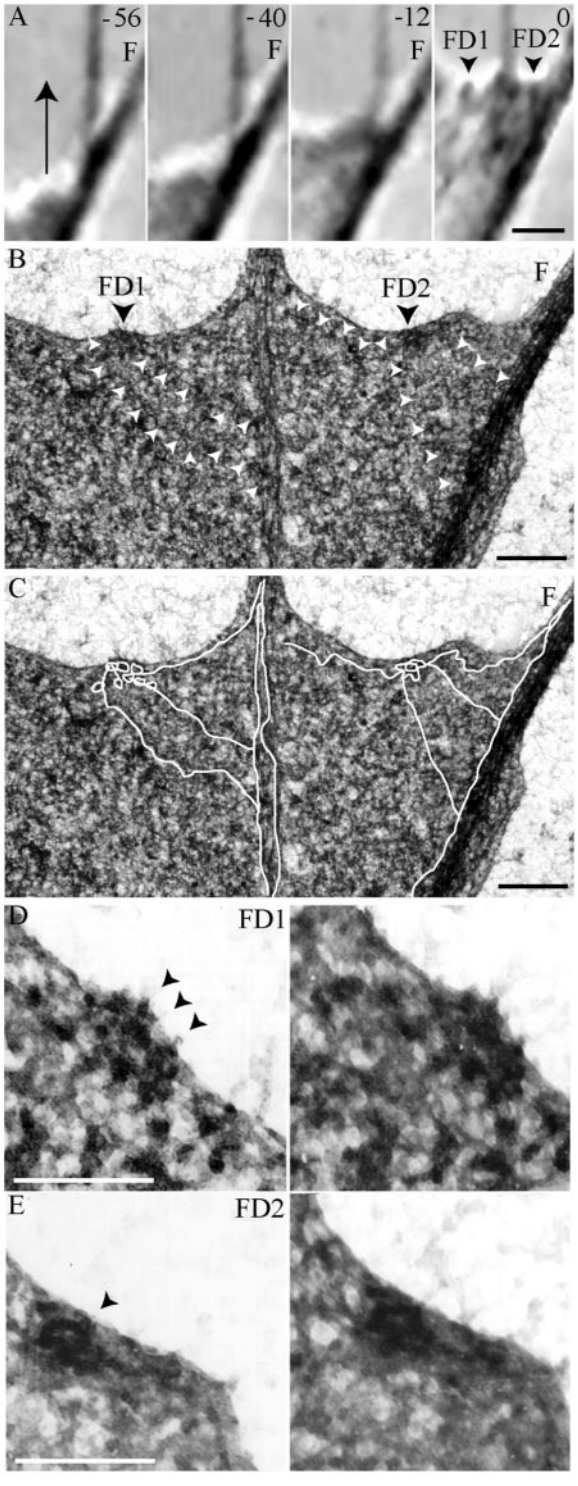

Figure 10. Correlative time lapse and EM reveal the emergence of marginal specializations and focal rings at basal adhesion sites. (A) Recordings document an extending veil (arrow) that developed two focal densities indicating basal adhesion sites (FD1, FD2), just before fixation. The mature filopodium on the right is engorged. Time before fixation is indicated in seconds at upper right. (B and C) The same region was identified in EM with the use of landmarks (compare with time 0 in A). This examination revealed that each focal density site corresponded to marginal specializations that radiated filaments. Some filaments are indicated by arrowheads in B and are outlined in C. Note the high electron density of the engorged filopodium (F). D and E) Stereo pairs at higher magnifications show the emergence of marginal densities and a focal ring. (D) At FD1, marginal electron densities were present, and the margin was tethered to the substrate (arrowheads). This morphology typifies the *initial adhesion phase*. (E) At FD2, a developing focal ring was tethered to the underlying substrate (arrowhead), whereas the margin was virtually free of tethers. This morphology typifies the *focal ring genesis phase*. Bars, A, 1 μm; B–E, 250 nm.

fail to support initiation in the absence of engorgement. One likely distinction between basal and other adhesions is the association of particular Rho family GTPases (reviewed in Hall, 1998), although the relation between such regulators, basal adhesion sites, and focal rings is currently unknown, and is one focus of our future research.

Basal adhesions appear to be vital to filopodial initiation, filopodial motility, and general stability. Filopodia have basal adhesions throughout their lifetime and regardless of their exact activity. These adhesions anchor the filopodial base, which generally remains stationary despite dynamic movements of the distal shaft (Argiro *et al.*, 1985; Bray and Chapman, 1985). If a basal adhesion is lost, the filopodium becomes unstable and commonly merges with an adjacent process that is adherent (Tosney and Balazovich, unpublished results), suggesting that basal adhesions are essential for counteracting tensions that can pull filopodia together, perhaps by transferring mechanical strains (Goldmann *et al.*, 1998). Basal adhesions may also be essential for maintaining growth cone form because, in addition to providing filopodial support, basal adhesions are associated with focal rings connecting actin bundles that underlie retracted and stable lamellar margins.

Focal Rings

In the model, focal rings arise at basal adhesions; nucleate actin filaments; link actin cytoskeleton to the adhesion site; and play vital roles in filopodial initiation, filopodial motility, and stability (Figure 12, B–E). Their development and association with stable adhesion sites is documented with the use of correlative time lapse-EM, and their association with actin filaments is confirmed by immuno-EM. They are visible with the use of a wide variety of preparatory regimens and so are not artifactual. They emerge at filopodial initiation sites, remain at filopodial bases and along filopodial shafts, and demark the maximum border for veil retraction.

Focal rings and their relation to adhesion and filopodial initiation have likely been unrecognized previously because ultrastructure was unlinked to motile events that forecast initiation, and because most such studies focused on lamellar rather than filopodial activities (Lewis and Bridgman, 1992; Small *et al.*, 1995; Svitkina and Borisy, 1999). Moreover, prior studies commonly used less optically accessible preparations or less revealing preparatory methods such as thin sectioning. For instance, freeze etch shows distinct particle patterns in the ventral surface of growth cones and fibroblasts (Lewis and Bridgeman, 1992; Samuelsson *et al.*, 1993)

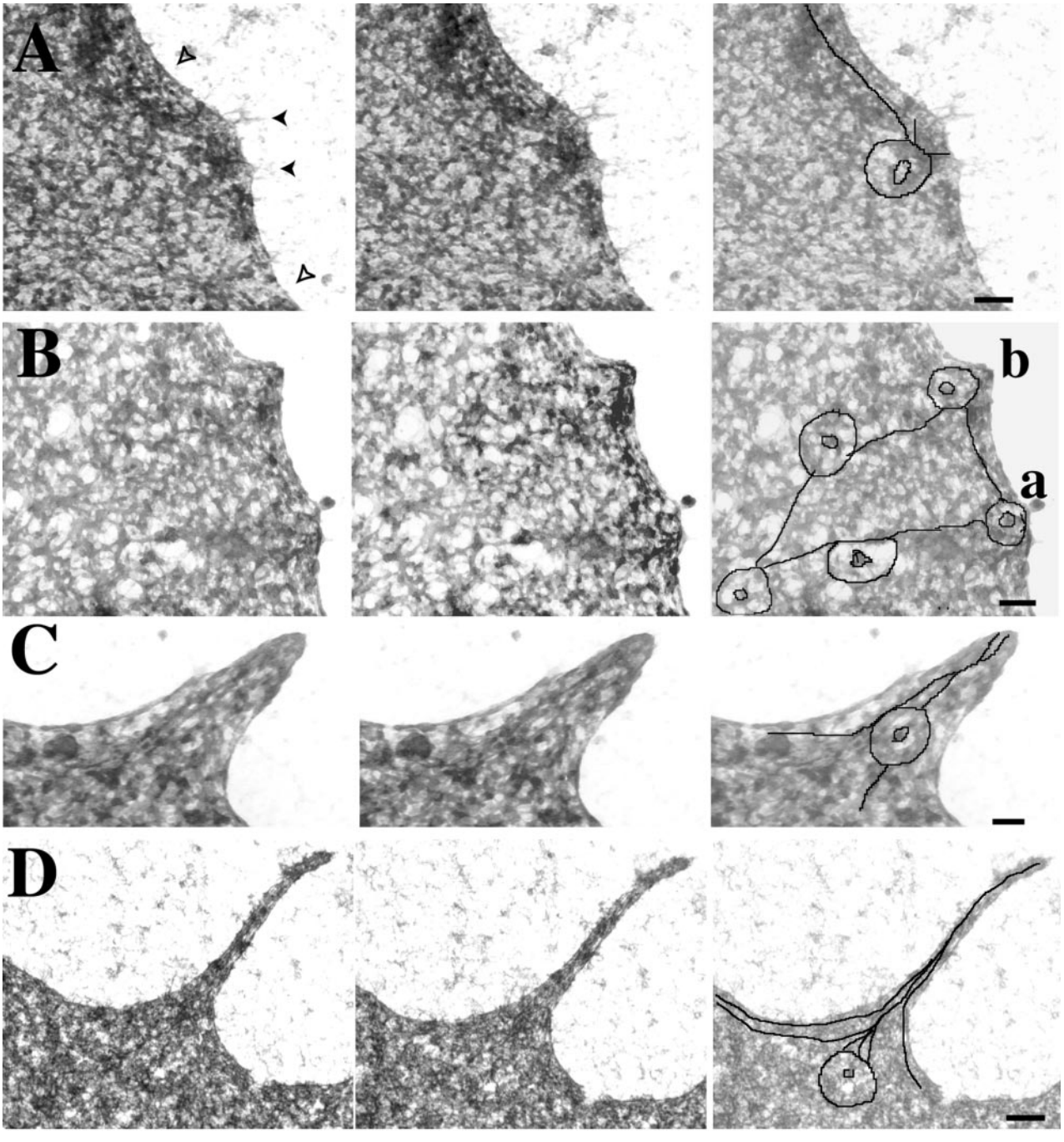

Figure 11. Nub maturation shows characteristic features. Nub genesis and morphogenesis were monitored in time lapse, and the same regions were then examined in EM. Left, stereo pairs; right, lower contrast image with some of the focal rings and filaments traced. (A–C) Nub genesis. As nubs emerge, the adjacent veil margins cease extension, and typical filament interconnections emerge. (A) Early in nub emergence, the margin had begun to extend past a focal ring and was free of the substrate (open arrowheads). In contrast, the focal ring appeared to be tethered to the substrate by membrane tethers (filled arrowheads). (B) Two nubs were forming at fixation. The less mature nub (a) showed the same features as in A. The margin edge lay slightly above the substrate, but the focal ring itself was close to the substrate and tethers connected it to the substrate. Later in nub emergence, at b, the margin distal to the focal ring was free of the substrate and lateral margins had begun to relax as the nub tip extended. Tracings highlight focal rings and interconnecting filaments. (C) In a nub that had fully emerged as a distinct projection with a wide base, the lateral veil margin had retreated proximally. Tracing highlights an axial filament connecting a focal ring to the nub tip, and a nub filament roughly paralleling the membrane. (D) Nub morphogenesis and filament bundling. Nub and axial filaments were bundled together in the more cylindrical portion of the nascent filopodium. At the filopodial base, axial filaments appeared to be caught in the act of bundling with nub filaments. Bars, 100 nm.

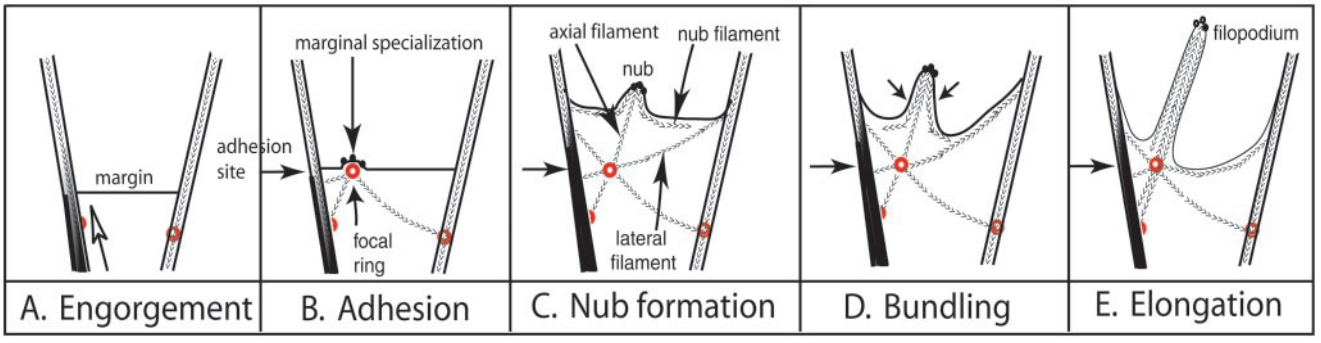

Figure 12. Model of events during filopodial initiation. Phases of filopodial initiation are schematized as new filopodia emerge from active lamellar extensions (veils) that extend between two mature filopodia. In the figure, the extending margin of a veil is indicated by a line between two mature filopodia. Actin filament polarities are indicated by >>>>>, representing the directions of barbed and pointed ends. A filopodial initiation complex comprises an engorging filopodium, a basal adhesion associated with a focal ring that radiates actin filaments, and a marginal specialization that will form the tip of the protruding nub and extending filopodium. In this model, focal rings mediate filament organization and substratum anchorage. (A) Engorgement. During extension of the veil margin, components essential for filopodial initiation are supplied as cytoplasm moves up a filopodial shaft (arrow), increasing the phase and electron density of the filopodium (black region in the left filopodium). (B) Adhesion. The veil margin adheres locally, developing a basal adhesion. At this persistent adhesion site (arrow), two types of specialization develop, a marginal specialization indicated by persistent electron densities (black dots), and a focal ring with radiating filaments. Both the marginal specializations and the focal ring are posited to act as nucleation sites. (C) Nub formation. The veil margin deadheres and continues to extend, but the focal ring remains at the basal adhesion site (arrow), providing anchorage. The focal ring nucleates filaments of two classes, axial and lateral. One or more axial filaments radiate between the focal ring and the marginal electron densities, and straighten as tension is generated between the extending margin and the anchored focal ring. Lateral filaments interconnect the focal ring with filament bundles and other focal rings, or end blindly within the veil. Nub filaments nucleate and extend from marginal specializations at the nub tip. As the mode of actin polymerization shifts from lamellar to filopodial, the veil ceases to advance. (D) Bundling. As the veil margin relaxes inward (arrows), the splayed nub filaments bundle about the axial filament, from distal to proximal. The actin bundles necessarily intersect the focal ring because bundling is oriented about the anchored axial filaments. Note that nub and axial filaments have opposite polarities. (E) Elongation. In an emergent filopodium, the actin bundle extends past the focal ring and intersects the engorged filopodium, commonly at a 30 degree angle that reflects architectural elements of the focal ring. Lateral filaments mark the proximal boundary for veil retreat, support the resulting lamellar margin, explain the parallel filament alignment underlying quiescent margins, and provide a scaffolding of interconnected filaments stabilized by anchored focal rings. Filopodial elongation ensues.

but retains so little cytoskeleton that detecting focal rings is problematic.

Nonetheless, structures similar to focal rings can be detected in published figures, suggesting that focal rings could be widely prevalent. For instance, we detected focal ring candidates (oblate donut-shaped structures ~120-nm maximum diameter) at filopodial bases from various cells processed in various ways: sensory growth cones prepared in another laboratory (Letourneau and Ressler, 1983, e.g., Figure 32; Lankford and Letourneau 1991, Figure 3f), retinal growth cones (Tsui *et al.*, 1983, Figure 5c), ciliary ganglion growth cones viewed in high voltage electron microscopy (Tosney and Wessells, 1983; Figures 2 and 8), keratinocytes (Vasioukhin *et al.*, 2000; Figure 2D) and fibroblasts (Evans *et al.* 1974, Figure 7D). However, oblate structures in the terminal web of intestinal brush borders (visualized with the use of quick-freeze, deep-etch rotary replication) intersected filaments regularly but had slightly larger dimensions (diameters: maximum, 131 ± 0.03 nm; minimum,108 ± 0.02 nm, n = 22; measured from figures in Hirokawa and Tilney, 1982; Mooseker *et al.*, 1984) and lacked a hollow core. Focal ring-like structures may also lie at origins of "intrapodia," actin-based protrusions that correlative time lapse-EM shows extend from a stable base proximal to the growth cone margin (Rochlin *et al.*, 1999, Figures 5B and 6A). Particularly because we also saw focal rings in Schwann cells, we expect that studies directly correlating filopodial initiation with ultrastructure will identify focal rings in many cell types.

Focal rings are ideally situated to modulate cytoskeletal tensions, because they are stationary, anchored to the substratum, and their radiating filaments interconnect multiple structures. The morphology of the radiating filaments suggests they are often under tension. Those that terminate on other structures are relatively straight, whereas those that end blindly are irregular. Tension could be generated mechanically simply because focal rings are stationary and termination sites are often moving, or by myosin-based contractility (Chrzanowska-Wodnicka and Burridge, 1996). Tension that depends on myosin-based contractility does maintain adhesions (Kaverina *et al.*, 1999; Rottner *et al.*, 1999), suggesting that those focal rings subject to the greatest tension would have the longest lifetimes.

Tensions among the cytoskeleton, the substratum, and the plasma membrane govern the ability of cells to change shape and protrude filopodia (Dai and Sheetz, 1995; Goldmann *et al.*, 1998; Karl and Bereiter-Hahn, 1999; Raucher and Sheetz, 2000). In growth cones, tension along actin filament bundles may direct engorgement during neurite initiation (Smith, 1994), orient microtubules in response to positive cues (Lin and Forscher, 1995), push growth cones forward (Heidemann and Bauxbaum, 1990), govern rates of growth cone advance (Heidemann, 1996), and help align filaments within filopodia (Tosney and Wessells, 1983). Tension central to

filopodial initiation could be generated along axial filaments and the nub filaments that bundle with them simply because axial filaments are anchored to the focal ring at the basal adhesion site, or because myosin isoforms are localized along axial and antiparallel nub filaments. This tension could generate the necessary force to overcome intrinsic membrane tensions (Raucher and Sheetz, 2000) and facilitate filament bundling by bringing filaments in close enough proximity to each other for actin cross-linking proteins, which mediate bundling (reviewed in Bartles, 2000), to bind to more than one filament at a time. If tension fails to generate along an emerging filopodial shaft then the shaft would probably be pushed back into the cell, as are unanchored filaments in other systems (Guild *et al.*, 1997). For instance, when filopodia contacting the inhibitory posterior sclerotome cells lose tension (indicated by their loss of rigidity), their filament bundle retracts proximally, out of the otherwise intact filopodium (Steketee and Tosney, unpublished results), as although tension was required to maintain, as well as to extend, an intact filopodium.

The structure of focal rings may also explain the common orientation of nascent filopodia relative to mature filopodia (Figure 12E). Focal rings often radiate filaments at 30 degree intervals, similar to the angle between emergent and parental filopodia. Two filopodia may even emanate from the same focal ring, since focal rings often lie at the vertex of filament bundles lying at about a 30 degree angle. The 30 degree angle (or its multiples) may be optimal because it is the most stable and allows the greatest tension to be developed along actin filament bundles.

Actin Nucleation, Elongation, and Bundling

The basal adhesions develop at the veil margin concurrently with at least two actin nucleation sites (Figure 12B). Not surprisingly, one nucleation site is represented by electron densities that emerge at the margin. Similar electron dense patches are known to generate actin filaments from tips of cellular processes in various cell types (reviewed in DeRosier and Tilney, 2000). They likely initiate filaments both in the nub and in mature filopodia. In mature filopodia, most filaments are oriented with their barbed ends distal, in accord with an origin and elongation from the tip (Lewis and Bridgeman, 1992).

A second site of nucleation is likely to be the focal ring. If radiating filaments nucleate from the focal ring then the axial filaments that extend between the focal ring and nub tip, and that come to lie at the core of filopodia, would have an opposite polarity to those filaments generated at the filopodial tip. This prediction is consistent with the reports of a minority population of filaments within growth cone filopodia that have reversed polarity (Lewis and Bridgeman, 1992). Lateral filaments, if they also nucleate from a focal ring, would have a similar polarity. Alternatively, filaments may nucleate elsewhere, and the focal ring, rather than serving as a nucleation center, may provide binding sites. In this scenario, axial filaments arise at the margin, whereas lateral filaments nucleate from mature filaments in associated filopodia. Nucleation from the sides of preexisting filaments via the ARP2/3 complex (Svitkina and Borisy, 1999) is consistent with the Y junction seen between lateral and mature filaments. However, the intersection angle alone is insufficient to implicate local nucleation, because it is also consistent with tension that could pull on an attached filament to create the Y-shaped profile. Filament polarity is targeted in a larger body of future work.

Regardless of the precise site where filaments nucleate, a novel and central element of the model is its proposition that filament bundling during initiation is guided by the axial filaments (Figure 12D). Because axial filaments are anchored at the basal adhesion site by the focal ring, and because they terminate at the nub tip, they form a stable element that could orient nub filament bundling. Once formed, the filament bundle would then necessarily intersect a stable adhesive site, the basal adhesion. Bundling itself is likely a product of actin cross-linking proteins that promote interactions among filaments and lateral interactions with the plasma membrane (Tilney *et al.*, 2000), possibly via members of the ezrin/radixin/moesin family (reviewed in Critchley, 2000), and membrane tensions also probably help to transform nubs into filopodia (Raucher and Sheetz, 2000). Filopodial emergence would thus require concerted processes: substrate anchorage, a supply of materials, actin polymerization that drives the filopodium outward and that continues throughout filopodial elongation, and bundling and lateral interactions with the membrane that facilitate transformation of the nub into a cylindrical filopodium (Bragina *et al.*, 1976; Edds, 1977; Katoh *et al.*, 1999). The guidance and anchorage required would be provided by axial filaments and focal rings.

ACKNOWLEDGMENTS

This study was supported by National Institutes of Health Grant NS-21308.

REFERENCES

Argiro, V., Bunge, M.B., and Johnson, M.I. (1985). A quantitative study of growth cone filopodial extension. J. Neurosci. Res *13*, 149–162.

Arregui, C.O., Carbonetto, S., and McKerracher, L. (1994). Characterization of neural cell adhesion sites: point contacts are the sites of interaction between integrins and the cytoskeleton in PC12 cells. J. Neurosci. *14*, 6967–6977.

Bartles, J. (2000). R., 2000. Parallel actin bundles and their multiple actin-bundling proteins. Curr. Opin. Cell Biol. *12*, 72–78.

Bastmeyer, M., and Stuermer, C.A. (1993). Behavior of fish retinal growth cones encountering chick caudal tectal membranes: a time-lapse study on growth cone collapse. J. Neurobiol. *24*, 37–50.

Bentley, D., and Toroian-Raymond, A. (1986). Disoriented pathfinding by pioneer neurone growth cones deprived of filopodia by cytochalasin treatment. Nature *323*, 712–715.

Bottenstein, J.E., Skaper, S.D., Varon, S. .S., and Sato, G.H. (1980). Selective survival of neurons from chick embryo sensory ganglionic dissociates utilizing serum-free supplemented medium. Exp. Cell Res. *125*, 183–190.

Bragina, E.E., Vasiliev, J.M., and Gelfand, I.M. (1976). Formation of bundles of microfilaments during spreading of fibroblasts on the substrate. Exp. Cell Res. *97*, 241–248.

Bray, D., and Chapman, K. (1985). Analysis of microspike movements on the neuronal growth cone. J. Neurosci. *5*, 3204–3213.

Castellano, F., Montcourrier, P., Guillemot, J.C., Gouin, E., Machesky, L., Cossart, P., and Chavrier, P. (1999). Inducible recruit-

ment of Cdc42 or WASP to a cell-surface receptor triggers actin polymerization and filopodium formation. Curr. Biol. *9*, 351–360.

Chien, C.B., Rosenthal, D.E., Harris, W.A., and Holt, C.E. (1993). Navigational errors made by growth cones without filopodia in the embryonic *Xenopus* brain. Neuron *11*, 237–251.

Chrzanowska-Wodnicka, M., and Burridge, K. (1996). Rho-stimulated contractility drives the formation of stress fibers and focal adhesions. J. Cell Biol. *133*, 1403–1415.

Clark, E.A., King, W.G., Brugge, J.S., Symons, M., and Hynes, R.O. (1998). Integrin-mediated signals regulated by members of the rho family of GTPases. J. Cell Biol. *142*, 573–586.

Cooper, J.A., and Schafer, D.A. (2000). Control of actin assembly and disassembly at filament ends. Curr. Opin. Cell Biol. *12*, 97–103.

Critchley, D.R. (2000). Focal adhesions – the cytoskeletal connection. Curr. Opin. Cell Biol. *12*, 133–139.

Dai, J., and Sheetz, M.P. (1995). Mechanical properties of neuronal growth cone membranes studied by tether formation with laser optical tweezers. Biophys. J. *68*, 988–996.

DeRosier, D.J., and Tilney, L.G. (2000). F-Actin bundles are derivatives of microvilli. What does this tell us about how bundles might form? J. Cell Biol. *148*, 1–6.

Edds, K.T. (1977). Dynamic aspects of filopodial formation by reorganization of microfilaments. J. Cell Biol. *73*, 479–491.

Evans, R.B., Morhenn, V., Jones, A.L., and Tomkins, G.M. (1974). Concomitant effects of insulin on surface membrane conformation and polysome profiles of serum-starved BALB/C 3t3 fibroblasts. J. Cell Biol. *61*, 95–106.

Fan, J., and Raper, J.A. (1995). Localized collapsing cues can steer growth cones without inducing their full collapse. Neuron *14*, 263–274.

Goldberg, D., and Burmeister, D. (1986). Stages in axon formation: observations of growth of *Aplysia* axons using video-enhanced contrast-differential interference contrast microscopy. J. Cell Biol. *103*, 1021–1031.

Goldmann, W.H., Galneder, R., Ludwig, M., Xu, W., Adamson, E.D., Wang, N., and Ezzell, R.M. (1998). Differences in elasticity of vinculin-deficient F9 cells measured by magnetometry and atomic force microscopy. Exp. Cell Res. *239*, 235–242.

Gomez, T.M., and Letourneau, P.C. (1994). Filopodia initiate choices made by sensory neuron growth cones at laminin/fibronectin borders in vitro. J. Neurosci. *14*, 5959–5972.

Guild, G.M., Connelly, P.S., Shaw, M.K., and Tilney, L.G. (1997). Actin filament cables in *Drosophila* nurse cells are composed of modules that slide passively past one another during dumping. J. Cell Biol. *138*, 783–797.

Hall, A. (1998). Rho GTPases and the actin cytoskeleton. Science *279*, 509–514.

Hamburger, V., and Hamilton, H.L. (1951). A series of normal stages in the development of the chick embryo. J. Morphol. *88*, 49–92.

Heidemann, S.R. (1996). Ctyoplasmic mechanisms of axonal and dendritic growth in neurons. Int. Rev. Cytol *165*, 235–296.

Heidemann, S.R., and Bauxbaum, R.E. (1990). Tension as a regulator and integrator of axonal growth. Cell Motil. Cytoskeleton *17*, 6–10.

Hirokawa, N., and Tilney, L.G. (1982). Interactions between actin filaments and between actin filaments and membranes in quick-frozen and deeply etched hair cells of the inner ear. J. Cell Biol. *95*, 249–261.

Katoh, K., Hammar, K., Smith, P.J.S., and Oldenbourg, R. (1999). Birefringence imaging directly reveals architectural dynamics of filamentous actin in living growth cones. Mol. Biol. Cell *10*, 197–210.

Karl, I., and Bereiter-Hahn, J. (1999). Tension modulates cell surface motility: a scanning acoustic microscopy study. Cell Motil. Cytoskeleton *43*, 349–359.

Kaverina, I., Krylyshkina, O., and Small, J.V. (1999). Microtubule targeting of substrate contacts promotes their relaxation and dissociation. J. Cell Biol. *146*, 1033–1044.

Lankford, K.L., and Letourneau, P. (1991). Roles of actin filaments and three second-messenger systems in short-term regulation of chick dorsal root ganglion neurite outgrowth. Cell Motil. Cytoskeleton *20*, 7–29.

Lee, J., and Jacobson, K. (1997). The composition and dynamics of cell-substratum adhesions in locomoting fish keratocytes. J. Cell Sci. *110*, 2833–2844.

Letourneau, P., and Ressler, A.H. (1983). Differences in the organization of actin in the growth cones compared with the neurites of culture neurons from chick embryos. J. Cell Biol. *97*, 963–973.

Lewis, A., and Bridgman, P. (1992). Nerve growth cone lamellipodia contain two populations of actin filaments that differ in organization and polarity. J. Cell Biol. *119*, 1219–1243.

Lin, C.H., and Forscher, P. (1995). Growth cone advance is inversely proportional to retrograde F-actin flow. Neuron *14*, 763–771.

Machesky, L.M., and Gould, K.L. (1999). The Arp2/3 complex: a multifunctional actin organizer. Curr. Opin. Cell Biol. *11*, 117–121.

Maupin, P., and Pollard, T.D. (1983). Improved preservation and staining of HeLa cells actin filaments, clathrin-coated membranes, and other cytoplasmic structures by tannic acid-glutaraldehyde-saponin fixation. J. Cell Biol. *96*, 51–62.

Meiri, K.F., and Burdick, D. (1991). Nerve growth factor stimulation of GAP-43 phosphorylation in intact isolated growth cones. J. Neurosci. *11*, 3155–3164.

Mooseker, M.A., Bonder, E.M., Conzelman, K.A., Fishkind, D.J., Howe, C.L., and Keller, T.C. (1984). Brush border cytoskeleton and integration of cellular functions. J. Cell Biol. *99*, 104s–112s.

Mullins, R.D., Heuser, J.A., and Pollard, T.D. (1998). The interaction of Arp2/3 complex with actin: nucleation, high affinity pointed end capping, and formation of branching networks of filaments. Proc. Natl. Acad. Sci. USA *95*, 6181–6186.

Oakley, R., and Tosney, K.W. (1993). Contact mediated mechanisms of motor axon segmentation. J. Neurosci. *13*, 3773–3792.

O'Connor, T.P., Duerr, J.S., and Bentley, D. (1990). Pioneer growth cone steering decisions mediated by single filopodial contacts in situ. J. Neurosci *10*, 3935–3946.

Raucher, D., and Sheetz, M.P. (2000). Cell spreading and lamellipodial extension rate is regulated by membrane tension. J. Cell Biol. *148*, 127–136.

Renaudin, A., Lehmann, M., Girault, J.-A., and McKerracher, L. (1999). Organization of point contacts in neuronal growth cones. J. Neurosci. Res *55*, 458–471.

Rochlin, M.W., Dailey, M.E., and Bridgman, P.C. (1999). Polymerizing microtubules activate site-directed F-actin assembly in nerve growth cones. Mol. Biol. Cell *10*, 2309–2327.

Rosner, H., and Fischer, H. (1996). In growth cones of rat cerebral neurons and human neuroblastoma cells, activation of protein kinase C causes a shift from filopodial to lamellipodial actin dynamics. Neurosci. Lett. *219*, 175–178.

Rottner, K., Hall, A., and Small, J.V. (1999). Interplay between Rac and Rho in the control of substrate contact dynamics. Curr. Biol. *9*, 640–648.

Samuelsson, S.J., Luther, P.W., Pumplin, D.W., and Bloch, R.J. (1993). Structures linking microfilament bundles to the membrane at focal contacts. J. Cell Biol. *122*, 485–496.

Schliwa, M., and van Blerkom, J. (1981). Structural integrity of cytoskeletal components. J. Cell Biol. *90*, 222–235.

Small, J.V., Herzog, M., and Anderson, K. (1995). Actin filament organization in the fish keratocyte lamellipodium. J. Cell Biol. *129*, 1275–1286.

Smith, C.L. (1994). Cytoskeletal movements and substrate interactions during initiation of neurite outgrowth by sympathetic neurons in vitro. J. Neurosci. *14*, 384–398.

Steketee, M.B., and Tosney, K.W. (1999). Contact with isolated sclerotome cells steers sensory growth cones by altering distinct elements of extension. J. Neurosci. *19*, 3495–3506.

Stossel, T.P., Hartwig, J.H., Janmey, P.A., and Kwiatkowski, D.J. (1999). Cell crawling two decades after Abercrombie. Biochem. Soc. Symp *65*, 267–280.

Svitkina, T.M., and Borisy, G.G. (1999). Arp 2/3 complex and actin depolymerizing factor/cofilin in dendritic organization and treadmilling of actin filament array in lamellipodia. J. Cell Biol. *145*, 1009–1026.

Svitkina, T.M., and Verkhovsky, A.B. (1995). Improved procedures for electron microscopic visulalization of the cytoskeleton of cultured cells. J. Struct. Biol. *115*, 290–303.

Svitkina, T.M., Verkjovsky, A.B., McQuade, K.M., and Borisy, G.G. (1997). Analysis of actin/myosin II system in fish epidermal keratinocytes: mechanism of cell body translocation. J. Cell Biol. *139*, 397–415.

Tilney, L.G., Tilney, M.S., and Guild, G.M. (1996a). Formation of actin filament bundles in the ring canals of developing *Drosophila* follicles. J. Cell Biol. *133*, 61–74.

Tilney, L.G., Connelly, P., Smith, S., and Guild, G.M. (1996b). F-actin bundles in *Drosophila* bristles are assembled from modules composed of short filaments. J. Cell Biol. *135*, 1291–1308.

Tilney, L.G., Connelly, P.S., Vranich, K.A., Shaw, M.K., and Guild, G.M. (1998). Why are two different cross-linkers necessary for actin bundle formation in vivo and what does each cross-link contribute? J. Cell Biol. *143*, 121–133.

Tilney, L.G., Connelly, P.S., Vranich, K.A., Shaw, M.K., and Guild, G.M. (2000). Regulation of actin filament cross-linking and bundle shape in *Drosophila* bristles. J. Cell Biol. *148*, 87–100.

Tosney, K.W., and Wessells, N.K. (1983). Neuronal motility: the ultrastructure of veils and microspikes correlates with their motile activities. J. Cell Sci. *61*, 389–411.

Tsui, H.C., Ris, H., and Klein, W.L. (1983). Ultrastructural networks in growth cones and neurites of cultured central nervous system neurons. Proc. Natl. Acad. Sci. USA *80*, 5779–5783.

Vasioukhin, V., Bauer, C., Yin, M., and Fuchs, E. (2000). Directed actin polymerization is the driving force for epithelial cell-cell adhesion. Cell *100*, 209–219.

Zheng, J.Q., Wan, J.J., and Poo, M.M. (1996). Essential role of filopodia in chemotropic turning of nerve growth cone induced by a glutamate gradient. J. Neurosci. *16*, 1140–1149.